Critical dynamics of a nonlocal model and critical behavior of perovskite manganites

Rohit Singh,[1,*] Kishore Dutta,[2,†] and Malay K. Nandy[1,‡]
[1]*Department of Physics, Indian Institute of Technology Guwahati, Guwahati 781 039, India*
[2]*Department of Physics, Handique Girls' College, Guwahati 781 001, India*
(Received 3 October 2015; revised manuscript received 20 April 2016; published 18 May 2016)

We investigate the nonconserved critical dynamics of a nonlocal model Hamiltonian incorporating screened long-range interactions in the quartic term. Employing dynamic renormalization group analysis at one-loop order, we calculate the dynamic critical exponent $z = 2 + \epsilon f_1(\sigma,\kappa,n) + O(\epsilon^2)$ and the linewidth exponent $w = -\sigma + \epsilon f_2(\sigma,\kappa,n) + O(\epsilon^2)$ in the leading order of ϵ, where $\epsilon = 4 - d + 2\sigma$, with d the space dimension, n the number of components in the order parameter, and σ and κ the parameters coming from the nonlocal interaction term. The resulting values of linewidth exponent w for a wide range of σ is found to be in good agreement with the existing experimental estimates from spin relaxation measurements in perovskite manganite samples.

DOI: 10.1103/PhysRevE.93.052132

I. INTRODUCTION

The nonequilibrium dynamics of magnetic systems near the critical point has received continual attention for decades [1–7]. In a typical scenario, the system is quenched near the critical temperature T_c at time $t = 0$ from an equilibrium state away from T_c. A sudden quench near T_c causes the system to undergo a slow relaxation towards the new equilibrium state, referred to as the critical slowing down. Theoretical models for the critical dynamics are usually based on a Langevin-type equation governed by the Ginzburg-Landau Hamiltonian for nonconserved or conserved order parameters [3–7]. These models elucidate the existence of various universality classes depending on the associated conservation laws and model parameters, namely the number of components n of the order parameter and the space dimensionality d. In addition to the two independent static critical exponents [e.g., the correlation length exponent ν defined via $\xi \propto |T - T_c|^{-\nu}$ and the Fisher exponent η for the algebraic decay of the two-point correlation function at criticality, $G(\mathbf{r} - \mathbf{r}') \propto |\mathbf{r} - \mathbf{r}'|^{-(d-2+\eta)}$], the order parameter relaxation is governed by a dynamic exponent z describing the critical slowing down. The characteristic time scale diverges as $\tau \propto |T - T_c|^{-z\nu}$ on approaching the transition point. Different values for z ensue depending on whether the order parameter is conserved and the existence of additional conserved quantities. The simplest cases among them are the purely relaxational models with either nonconserved (Model A) or conserved (Model B) order parameter Φ. The renormalization group (RG) treatment for model A with short-range (SR) interactions gives $z = 2 + c\eta$ at two-loop order with $c = 6\ln(\frac{4}{3}) - 1$, yielding $z = 1.984$ in three dimensions [4–6].

While the above theoretical investigations were carried out for the model A with SR interactions, a long-range (LR) model was proposed by Fisher, Ma, and Nickel [8] where the quadratic term in the model Hamiltonian was modified by incorporating LR interactions. Following this (LR) model, the corresponding nonconserved critical dynamics was investigated by Belim [9] in a field-theoretic framework. Carrying out the calculations at two-loop order and employing the Padé-Borel resummation technique, it was found that the LR interaction affects the relaxation time of the system, indicated by the variation of z within the range $2.000072 \leqslant z \leqslant 2.006628$.

Recently, the doped perovskite manganites [$(R_{1-x}A_xMnO_3)$, R stands for rare-earth and A stands for alkaline-earth elements] have become the focus of scientific and technological interest as they exhibit colossal magnetoresistance (CMR) [10–14]. A number of experimental investigations on the critical slowing down of such compounds near the paramagnetic (PM) to ferromagnetic (FM) phase transition were performed via a number of powerful techniques, namely muon spin relaxation (μSR) spectroscopy [15,16], inelastic neutron scattering [17], pump-probe method [18,19], and magnetic resonance methods [20,21]. In some of these experiments [18,19] the relaxation time exponent νz was measured for thin-film samples while in some other experiments [16,20,21], the linewidth exponent $w = \nu(z + 2 - d - \eta)$ [4,22] was measured for bulk samples. In Ref. [16], μSR measurements were performed on a single crystal of $Nd_{0.5}Sr_{0.5}MnO_3$ exhibiting critical slowing down of Mn ion spin fluctuations in the critical paramagnetic regime. This facilitated the measurement of the linewidth exponent w from the relaxation of the diffusive component, yielding $w = 0.59 \pm 0.05$. Using the electron-paramagnetic resonance (EPR) technique, Atsarkin *et al.* [20] investigated the critical slowing down of longitudinal spin relaxation close to the PM-FM phase transition temperature T_c in $La_{1-x}Ca_xMnO_3$ for $x = 0.2$, 0.25, and 0.33. From the magnetic resonance linewidth measurements, they obtained the linewidth exponent $w \approx 0.5$ for all samples. Using a similar experimental technique, Yassin *et al.* [21] measured w for $La_{0.67-2x}Nd_{2x}Ca_{0.33-x}Sr_xMnO_3$ with $x = 0$, 0.1, 0.15, 0.2, and 0.25 and found w to be nearly a constant ($\approx$0.5) for all samples. The above spin relaxation experiments [16,20,21] indicate an interesting feature of perovskite manganite samples in the sense that the linewidth exponent w near the critical point of PM-FM phase transition is close to $w \approx 0.5$ independent of their chemical compositions (x, R, and A).

Microscopic models for the magnetic (and electrical) properties of perovskite manganites are based on the framework

*rohit.singh@iitg.ernet.in
†kdkishore77@gmail.com
‡mknandy@iitg.ernet.in

of double exchange (DE) interaction [10,13,23] and electron-phonon coupling, partially the Jahn-Teller type [10,24], leading to polaron formation. It is interesting to note that the polaron model correctly explains the insulating (paramagnetic) phase in these systems and it has been suggested [25] that the polaron effect switches off as temperature is lowered through T_c to obtain a metallic (ferromagnetic) phase. However, as discussed in Refs. [20,21], the experimental finding that the linewidth exponent w remains constant for different samples (namely $w \approx 0.5$) is not consistent with the prediction of the polaron hopping model [26,27]. In addition, Monte Carlo (MC) simulations have been performed [28–32] on a model Hamiltonian representing the DE interaction for the investigation of the static as well as dynamic critical behavior. These simulations yield $\nu = 0.6949 \pm 0.0038$, $\beta = 0.3535 \pm 0.0030$, $\gamma = 1.3909 \pm 0.0030$ in Ref. [28], $\beta \approx 0.365$ in Refs. [29,31], $\beta = 0.36 \pm 0.01$ in Ref. [30], and $\nu = 0.686 \pm 0.010$, $\beta = 0.356 \pm 0.006$, $z = 1.975 \pm 0.010$ in Ref. [32], that are close to those of the three-dimensional (3D) Heisenberg model (with SR interaction). This suggests that the DE and 3D Heisenberg models [33,34] belong to the same universality class. Although a few perovskite manganite samples [35,36] are found to have 3D Heisenberg critical indices, a vast majority of samples [11,37–41] exhibit a widely varying sets of critical indices including the tricritical mean-field exponents. Thus, although the DE is widely accepted as one of the key mechanisms for CMR in perovskite manganites, models involving the DE interaction cannot capture their widely varying critical behavior near the PM-FM phase transition. Further, theoretical developments along the lines of the SR TDGL model [6] and its modified LR version [9] cannot be expected to reproduce their widely varying critical indices. This necessitates an alternative model capable of capturing the static as well as the dynamic critical exponents observed in experimental samples.

Lattice distortions are known to be important in perovskite manganites as they are coupled to electronic, magnetic, and chemical degrees of freedom [10,42–44]. A pronounced variation of electrical resistivity and a large shift of T_c after isotope exchange (^{18}O for ^{16}O) indicate a strong spin-lattice coupling [12,45]. It has been pointed out [10,46,47] that lattice distortions are directly related to the imposed strain due to perturbations induced via changes in R, A, and x. A quantitative analysis [46] predicted a dramatic sensitivity of material properties to strain, particularly the shifting of T_c with strain. Different strain modes are shown to evolve depending on whether the perturbation is due to the size distribution of R/A atoms or to the change in the doping concentration x. It may further be stated that elastic interactions play an essential role in the formation of superstructures [48] and texturing [47] observed in perovskite manganites.

It is interesting to note that, a number of theoretical investigations have been performed on the role of spin-lattice coupling near the critical point. In particular, Fisher [49] considered a compressible Ising system with spin-lattice coupling resulting from the fact that the exchange interaction varies with the separation between the spins. Wagner [50,51] reconsidered the problem and obtained an effective Hamiltonian involving a long-range four spin interaction term as a result of the spin-lattice coupling. Aharony considered a continuum generalization of this model [52] with wave-vector-dependent four-spin (quartic) coupling and showed the existence of tricriticality in the system. It is important to note that some perovskite manganite samples exhibit triciritcal exponents. At the same time, spin-lattice interactions are known to play an important role in perovskite manganites. Thus, any model describing the critical properties of perovskite manganite samples should include the effect of spin-lattice coupling and it should be able to exhibit tricriticality in the system. Theoretical investigations described above indicate that the quartic term in the effective Hamiltonian should have a long-range (nonlocal) character as a result of spin lattice interaction. Thus it is interesting to consider a long-range model Hamiltonian with nonlocal interaction in the quartic term and see whether such a model can exhibit the critical properties of perovskite manganite samples including tricriticality.

The static critical behavior of a model Hamiltonian with a nonlocal interaction in the quartic term was studied recently by means of Wilson's momentum shell decimation RG scheme [53]. Quite satisfactorily, this nonlocal model was found to represent a variety of critical exponents corresponding to the static critical behavior of a wide range of perovskite manganite samples including triciritcal exponents exhibited by some of the samples. This motivates us to investigate the dynamic critical behavior governed by the same nonlocal model Hamiltonian in the spirit of Model A of Halperin and Hohenberg [6]. Through this nonlocal mode Hamiltonian, we are particularly interested in capturing the dynamic critical behavior of perovskite manganites near the PM-FM phase transition.

In this paper, we write the nonconserved Langevin dynamics for the order parameter Φ governed by the nonlocal model Hamiltonian. Employing Wilson's momentum shell decimation RG scheme, we carry out the calculations at one-loop order and obtain the dynamic exponent z and the linewidth exponent w in the leading order of ϵ, where $\epsilon = 4 - d + 2\sigma$, with d the space dimension and σ is a parameter occurring in the nonlocal interaction term. Interestingly, the linewidth exponent w is found to be almost constant ($w \approx 0.5$), although the static critical exponents vary with the nonlocal exponent σ in the range $-0.5 \leqslant \sigma \leqslant 0$. The critical exponents agree well with the available experimental estimates for different samples. This suggests that the nonlocal model Hamiltonian is a viable model for the critical behavior of PM-FM phase transition in perovskite manganites.

The rest of the paper is organized as follows. In Sec. II, we introduce the dynamical model in the presence of nonlocal interactions and present the analytical results following from the dynamic RG analysis. Section III presents a comparison of the predicted results with the experimental estimates. Finally, discussions and conclusions are given in Sec. IV.

II. NONLOCAL UNCONSERVED DYNAMICS AND RG CALCULATIONS

The dynamics of an n-component unconserved order parameter $\phi_i(\mathbf{x},t)$ is given by [4,6]

$$\frac{\partial}{\partial t}\phi_i(\mathbf{x},t) = -\Gamma_0 \frac{\delta H}{\delta \phi_i(\mathbf{x},t)} + \eta_i(\mathbf{x},t), \tag{1}$$

where we incorporate nonlocal interactions in the quartic term of the Ginzburg-Landau (GL) free-energy functional H as

$$H[\Phi] = \int d^d x \left[\frac{c_0}{2} |\nabla \Phi(\mathbf{x})|^2 + \frac{r_0}{2} \Phi^2(\mathbf{x}) + \int d^d x' \Phi^2(\mathbf{x}) u(\mathbf{x}-\mathbf{x}') \Phi^2(\mathbf{x}') \right], \tag{2}$$

where d is the space dimension, the time dependence has been suppressed for brevity, and $\Phi^2 = \sum_{i=1}^n \phi_i^2$, $|\nabla\Phi|^2 = \sum_{i=1}^n \nabla\phi_i \cdot \nabla\phi_i$, and $u(\mathbf{x}-\mathbf{x}')$ is the nonlocal coupling function. The term $\eta_i(\mathbf{x},t)$ represents a Gaussian white noise with zero mean and correlation

$$\langle \eta_i(\mathbf{k},\omega)\eta_j(\mathbf{k}',\omega')\rangle = 2\Gamma_0 (2\pi)^{d+1} \delta^d(\mathbf{k}+\mathbf{k}')\delta(\omega+\omega')\delta_{ij} \tag{3}$$

in the Fourier space. Equation (1) can be portrayed in the Fourier space as

$$\left[\frac{-i\omega}{\Gamma_0} + r_0 + c_0 k^2\right]\phi_i(\mathbf{k},\omega) = \frac{\eta_i(\mathbf{k},\omega)}{\Gamma_0} - 4\int \frac{d^d k_1}{(2\pi)^d}\frac{d\omega_1}{2\pi}\int \frac{d^d k_2}{(2\pi)^d}\frac{d\omega_2}{2\pi} u(\mathbf{k}_1-\mathbf{k}) \times \phi_i(\mathbf{k}_1,\omega_1)\phi_j(\mathbf{k}_2,\omega_2)\phi_j(\mathbf{k}-\mathbf{k}_1-\mathbf{k}_2,\omega-\omega_1-\omega_2), \tag{4}$$

where summation over repeated indices is implied. We start with Eq. (4) and perform a dynamic RG analysis [6,7,54] at one-loop order. Decimation of scales from the momentum shell lying in the range $\frac{\Lambda}{b} \leqslant k \leqslant \Lambda$ (Λ being the ultraviolet cutoff) yields the equation of motion in the reduced range $0 \leqslant k \leqslant \frac{\Lambda}{b}$ as

$$\phi_i(\mathbf{k},\omega) = G_0(\mathbf{k},\omega)\frac{\eta_i(\mathbf{k},\omega)}{\Gamma_0} - 4G_0(\mathbf{k},\omega)\int \frac{d^d k_1}{(2\pi)^d}\frac{d\omega_1}{2\pi} \times \int \frac{d^d k_2}{(2\pi)^d}\frac{d\omega_2}{2\pi} u(\mathbf{k}_1-\mathbf{k})\phi_i(\mathbf{k}_1,\omega_1) \times \phi_j(\mathbf{k}_2,\omega_2)\phi_j(\mathbf{k}-\mathbf{k}_1-\mathbf{k}_2,\omega-\omega_1-\omega_2) + G_0(\mathbf{k},\omega)R_i(\mathbf{k},\omega), \tag{5}$$

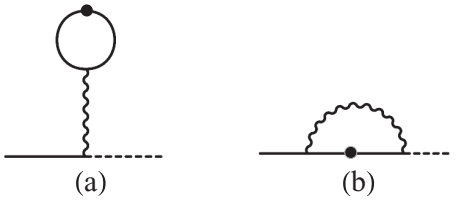

FIG. 1. One-loop Feynman diagrams corresponding to the self-energies (a) Σ_a and (b) Σ_b. Solid lines represent the propagator G_0, dashed lines the field ϕ_i, dots the noise correlation, and wiggly lines represent the nonlocal coupling $u(\mathbf{k})$.

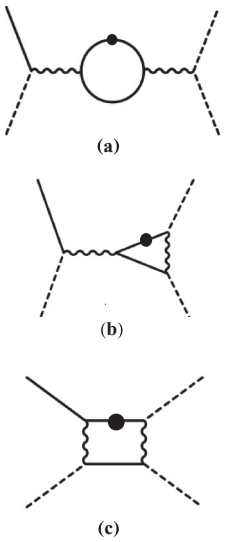

FIG. 2. One-loop Feynman diagrams for the vertex $u(\mathbf{k}_1-\mathbf{k})$. Panels (a), (b), and (c) correspond to Υ_a, Υ_b, and Υ_c given in Eqs. (13)–(15). The various lines and the dots have the same meanings as in Fig. 1.

where $G_0(\mathbf{k},\omega) = \left(\frac{-i\omega}{\Gamma_0} + r_0 + c_0 k^2\right)^{-1}$ is the bare propagator, and

$$R_i(\mathbf{k},\omega) = -(\Sigma_a + \Sigma_b)\phi_i(\mathbf{k},\omega),$$

with the self-energy corrections (Fig. 1)

$$\Sigma_a(\mathbf{k},\omega) = \frac{8n}{\Gamma_0}\int \frac{d^d k_1}{(2\pi)^d}\frac{d\omega_1}{2\pi} u(\mathbf{0})|G_0(\mathbf{k}_1,\omega_1)|^2, \tag{6}$$

$$\Sigma_b(\mathbf{k},\omega) = \frac{16}{\Gamma_0}\int \frac{d^d k_1}{(2\pi)^d}\frac{d\omega_1}{2\pi} u(\mathbf{k}_1-\mathbf{k})|G_0(\mathbf{k}_1,\omega_1)|^2, \tag{7}$$

at one-loop order. We choose the form of the coupling function to be the same as that of the static case [53] as

$$u(\mathbf{q}) = \frac{\lambda_0}{[\mathbf{q}^2+m^2]^\sigma} \tag{8}$$

in the Fourier space, where λ_0 is a coupling constant and m is a screening parameter. Performing the frequency and momentum integrations appearing in Eqs. (6) and (7), we obtain

$$\Sigma_a(\mathbf{0},0) = \frac{4nS_d\lambda_0}{c_0 m^{2\sigma}[2\pi]^d} \times \left[\left(\frac{b^{2-d}-1}{2-d}\right)\Lambda^{d-2} - \frac{r_0}{c_0}\left(\frac{b^{4-d}-1}{4-d}\right)\Lambda^{d-4}\right], \tag{9}$$

$$\Sigma_b(\mathbf{0},0) = \frac{8S_d\lambda_0}{c_0[2\pi]^d}\left[\left(\frac{b^{2-d+2\sigma}-1}{2-d+2\sigma}\right)\Lambda^{d-2-2\sigma} - \left(\frac{r_0}{c_0}+\sigma m^2\right)\left(\frac{b^{4-d+2\sigma}-1}{4-d+2\sigma}\right)\Lambda^{d-4-2\sigma}\right] + \frac{8S_d\lambda_0}{c_0[2\pi]^d}k^2\left[\frac{\sigma(2\sigma+2-d)}{d}\left(\frac{b^{4-d+2\sigma}-1}{4-d+2\sigma}\right)\Lambda^{d-4-2\sigma}\right], \tag{10}$$

in the large-scale and long-time limits ($k \to 0, \omega \to 0$), where $S_d = 2\pi^{d/2}/\Gamma(d/2)$ is the surface area of a unit sphere embedded in a d-dimensional space. These expressions for self-energy give rise to corrections Δr and Δc to the bare coefficients r_0 and c_0 as

$$\Delta r = \frac{4nS_d\lambda_0}{c_0 m^{2\sigma}[2\pi]^d}\left[\left(\frac{b^{2-d}-1}{2-d}\right)\Lambda^{d-2} - \frac{r_0}{c_0}\left(\frac{b^{4-d}-1}{4-d}\right)\Lambda^{d-4}\right] + \frac{8S_d\lambda_0}{c_0[2\pi]^d}\left[\left(\frac{b^{2-d+2\sigma}-1}{2-d+2\sigma}\right)\Lambda^{d-2-2\sigma} - \left(\frac{r_0}{c_0}+\sigma m^2\right)\left(\frac{b^{4-d+2\sigma}-1}{4-d+2\sigma}\right)\Lambda^{d-4-2\sigma}\right], \tag{11}$$

and

$$\Delta c = \frac{8\sigma(2\sigma+2-d)S_d\lambda_0}{c_0 d[2\pi]^d}\left(\frac{b^{4-d+2\sigma}-1}{4-d+2\sigma}\right)\Lambda^{d-4-2\sigma}. \tag{12}$$

We see that the noise amplitude Γ_0 does not acquire any correction at this order of calculations.

Within the same calculational framework, we also obtain the relevant corrections to the bare vertex $u(\mathbf{k}_1 - \mathbf{k})$ (Fig. 2) at one-loop order and obtain

$$\Upsilon_a = \frac{64n}{\Gamma_0}\int\frac{d^dk_1d\omega_1}{[2\pi]^{d+1}}\int\frac{d^dk_2d\omega_2}{[2\pi]^{d+1}}u(\mathbf{k}_1-\mathbf{k})\phi_i(\mathbf{k}_1,\omega_1)\phi_j(\mathbf{k}_2,\omega_2)\phi_j(\mathbf{k}-\mathbf{k}_1-\mathbf{k}_2,\omega-\omega_1-\omega_2) \times \int\frac{d^dpd\Omega}{[2\pi]^{d+1}}u(\mathbf{k}_1-\mathbf{k})|G_0(\mathbf{p},\Omega)|^2G_0(\mathbf{k}-\mathbf{k}_1-\mathbf{p},\omega-\omega_1-\Omega), \tag{13}$$

$$\Upsilon_b = \frac{256}{\Gamma_0}\int\frac{d^dk_1d\omega_1}{[2\pi]^{d+1}}\int\frac{d^dk_2d\omega_2}{[2\pi]^{d+1}}u(\mathbf{k}_1-\mathbf{k})\phi_i(\mathbf{k}_1,\omega_1)\phi_j(\mathbf{k}_2,\omega_2)\phi_j(\mathbf{k}-\mathbf{k}_1-\mathbf{k}_2,\omega-\omega_1-\omega_2) \times \int\frac{d^dpd\Omega}{[2\pi]^{d+1}}u(\mathbf{p}-\mathbf{k}+\mathbf{k}_1+\mathbf{k}_2)|G_0(\mathbf{p},\Omega)|^2G_0(\mathbf{k}-\mathbf{k}_1-\mathbf{p},\omega-\omega_1-\Omega), \tag{14}$$

$$\Upsilon_c = \frac{256}{\Gamma_0}\int\frac{d^dk_1d\omega_1}{[2\pi]^{d+1}}\int\frac{d^dk_2d\omega_2}{[2\pi]^{d+1}}\phi_i(\mathbf{k}_1,\omega_1)\phi_j(\mathbf{k}_2,\omega_2)\phi_j(\mathbf{k}-\mathbf{k}_1-\mathbf{k}_2,\omega-\omega_1-\omega_2) \times \int\frac{d^dpd\Omega}{[2\pi]^{d+1}}u(\mathbf{p}-\mathbf{k})u(\mathbf{p}-\mathbf{k}_1)|G_0(\mathbf{p},\Omega)|^2G_0(\mathbf{k}_1+\mathbf{k}_2-\mathbf{p},\omega_1+\omega_2-\Omega). \tag{15}$$

Performing the loop integrations appearing in the above expressions for Υ_a and Υ_b, we obtain the correction $\Delta\lambda$ to λ_0 as

$$\Delta\lambda = -\frac{4nS_d\lambda_0^2}{c_0^2 m^{2\sigma}[2\pi]^d}\left[\left(\frac{b^{4-d}-1}{4-d}\right)\Lambda^{d-4} - \frac{2r_0}{c_0}\left(\frac{b^{6-d}-1}{6-d}\right)\Lambda^{d-6}\right] - \frac{16S_d\lambda_0^2}{c_0^2[2\pi]^d}\left[\left(\frac{b^{4-d+2\sigma}-1}{4-d+2\sigma}\right)\Lambda^{d-4-2\sigma} - \left(\sigma m^2+\frac{2r_0}{c_0}\right)\left(\frac{b^{6-d+2\sigma}-1}{6-d+2\sigma}\right)\Lambda^{d-6-2\sigma}\right] \tag{16}$$

in the $k \to 0, \omega \to 0$ limit. Υ_c being irrelevant, it does not contribute to $\Delta\lambda$.

The RG calculations is carried out by maintaining the form of the original equation [Eq. (4)] invariant. Consequently, the reduced range $0 \leqslant k \leqslant \frac{\Lambda}{b}$ is projected into the full range ($0 \leqslant k \leqslant \Lambda$) by rescaling the variables and the field as $k' = bk, \omega' = b^z\omega$, and $\Phi' = b^x\Phi$. These, together with the assumption of self-similarity and powerlike fall-off of the correlation function at the critical point [8,55,56], yield $\Gamma' = b^{z-2+\eta}(\Gamma_0 + \Delta\Gamma)$, $\lambda' = b^{4-d+2\sigma-2\eta}(\lambda_0 + \Delta\lambda)$, $r' = b^{2-\eta}(r_0 + \Delta r)$, and $c' = b^{-\eta}(c_0 + \Delta c)$. Thus, incorporating the renormalized corrections to r_0, c_0, and λ_0 given by Eqs. (11), (12), and (16), we obtain the RG flow equations as

$$r' = b^{2-\eta}\left[r_0 + \frac{4n\lambda_0 S_d}{m^{2\sigma}[2\pi]^d}\left\{\frac{(b^{2-d}-1)\Lambda^{d-2}}{c_0(2-d)} - \frac{r_0}{c_0^2}\frac{(b^{4-d}-1)\Lambda^{d-4}}{(4-d)}\right\} + \frac{8\lambda_0 S_d}{[2\pi]^d}\left\{\frac{(b^{2\sigma+2-d}-1)\Lambda^{d-2\sigma-2}}{c_0(2\sigma+2-d)} - \left(\frac{r_0}{c_0^2}+\frac{\sigma m^2}{c_0}\right)\frac{(b^{2\sigma+4-d}-1)\Lambda^{d-2\sigma-4}}{(2\sigma+4-d)}\right\}\right], \tag{17}$$

$$\lambda' = b^{4-d-2\eta+2\sigma}\Bigg[\lambda_0 - \frac{4n\lambda_0^2}{m^{2\sigma}}\frac{S_d}{[2\pi]^d}\Bigg\{\frac{(b^{4-d}-1)\Lambda^{d-4}}{c_0^2(4-d)} - \frac{2r_0}{c_0^3}\frac{(b^{6-d}-1)\Lambda^{d-6}}{(6-d)}\Bigg\}$$
$$-\frac{16\lambda_0^2 S_d}{[2\pi]^d}\Bigg\{\frac{(b^{4-d+2\sigma}-1)\Lambda^{d-4-2\sigma}}{c_0^2(4-d+2\sigma)} - \left(\frac{\sigma m^2}{c_0^2}+2\frac{r_0}{c_0^3}\right)\frac{(b^{6-d+2\sigma}-1)\Lambda^{d-6-2\sigma}}{(6-d+2\sigma)}\Bigg\}\Bigg], \tag{18}$$

$$c' = b^{-\eta}\Bigg[c_0 + \frac{8\sigma(2-d+2\sigma)\lambda_0 S_d}{d[2\pi]^d}\Bigg\{\frac{(b^{4-d+2\sigma}-1)\Lambda^{d-4-2\sigma}}{c_0(4-d+2\sigma)}\Bigg\}\Bigg], \tag{19}$$

$$\Gamma' = b^{z-2+\eta}\Gamma_0. \tag{20}$$

These RG flow equations suggest the existence of a LR fixed point $r \to r^*$, $\lambda \to \lambda^*$, $c \to c^* = c$, and $\Gamma_0 \to \Gamma_0^* = \Gamma_0$, corresponding to

$$\frac{r^*}{c} = -\frac{(4-d-2\eta+2\sigma)\left\{\frac{n}{\kappa^\sigma}+2(1-\sigma\kappa)\right\}\Lambda^2}{(2-\eta)\left\{\frac{n}{\kappa^\sigma}+4(1-\sigma\kappa)\right\} - (4-d-2\eta+2\sigma)\left(\frac{n}{\kappa^\sigma}+2\right)} \tag{21}$$

and

$$\frac{\lambda^*}{c^2} = \frac{(4-d-2\eta+2\sigma)\Lambda^{4-d+2\sigma}}{\frac{S_d}{(2\pi)^d}\left\{\frac{4n}{\kappa^\sigma}+16(1-\sigma\kappa)\right\}}, \tag{22}$$

where $\kappa = m^2/\Lambda^2$ is a redefined screening parameter. A linear stability analysis indicates that the above fixed point is stable for values of σ lying in the range $-0.5 \leqslant \sigma \leqslant 0.5$ in three dimensions. Further, the upper critical dimension d_c turns out to be $d_c = 4 + 2\sigma$. From Eq. (19), the Fisher exponent η can be calculated in the leading order of $\epsilon = d_c - d$ as

$$\eta = -\frac{2\sigma\epsilon}{(\sigma+2)\left[\frac{n}{\kappa^\sigma}+4(1-\sigma\kappa)\right]-4\sigma} + O(\epsilon^2). \tag{23}$$

Equation (20) yields the dynamic critical exponent z as $z = 2 - \eta$, giving

$$z = 2 + \frac{2\sigma\epsilon}{(\sigma+2)\left[\frac{n}{\kappa^\sigma}+4(1-\sigma\kappa)\right]-4\sigma} + O(\epsilon^2). \tag{24}$$

Thus, we find $z = 2 + \epsilon f_1(\sigma,\kappa,n) + O(\epsilon^2)$. In Fig. 3, we display the variations of z with (a) order parameter components n and (b) screening parameter κ in the physically allowed range of σ in three dimensions. In Fig. 3(a), we show the variations of z with n for $\kappa = 0.001$ while in Fig. 3(b) we show the variation of z with κ for $n = 3$. These plots clearly show that the dynamic exponent z undergoes negligible variation with respect to n and κ in the negative regime of σ.

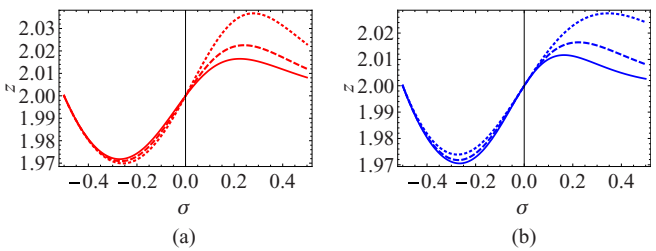

FIG. 3. Plots for $z = 2 + \epsilon f_1(\sigma,\kappa,n) + O(\epsilon^2)$. Panel (a) shows the variation of z with n for $\kappa = 0.001$ and panel (b) shows the variation of z with κ for $n = 3$ in $d = 3$. The dotted, dashed, and solid curves correspond to $n = 1,2,3$ in (a) and $\kappa = 0.0001,0.001,0.01$ in (b).

It may be noted that, similarly to the original model A dynamics with SR Φ^4 potential, the present LR model does not give any relevant RG corrections to the noise amplitude Γ_0 at one-loop order. However, due to the incorporation of nonlocal coupling function $u(\mathbf{k})$, we obtain a nonzero correction to η at one-loop order in the leading order of ϵ. Thus, it is the renormalization of η that leads to strikingly different long-range dependent results for the dynamic exponent z. We find that the value of z lies in the range $1.972 \leqslant z \leqslant 2.016$ for $d = 3$. This may be compared with the field-theoretic result $2.000072 \leqslant z \leqslant 2.006628$ [9] obtained from a different model.

In order to calculate the linewidth exponent w, given by the scaling relation $w = \nu(z+2-d-\eta) = \nu(4-d-2\eta)$, we calculate the correlation length exponent ν and obtain

$$\nu = \frac{1}{2} + \frac{\epsilon\left(\frac{n}{\kappa^\sigma}+2\right)}{2\left[\frac{n}{\kappa^\sigma}+4(1-\sigma\kappa)\right]} \times\left\{\frac{1}{2} + \frac{2\sigma}{(\sigma+2)\left[\frac{n}{\kappa^\sigma}+4(1-\sigma\kappa)\right]-4\sigma}\right\} - \frac{\sigma\epsilon}{2(\sigma+2)\left[\frac{n}{\kappa^\sigma}+4(1-\sigma\kappa)\right]-8\sigma} + O(\epsilon^2). \tag{25}$$

Equation (25) together with Eq. (23) yields

$$w = -\sigma + \epsilon\Bigg[\frac{1}{2} + \frac{\sigma}{(\sigma+2)\left\{\frac{n}{\kappa^\sigma}+4(1-\sigma\kappa)\right\}-4\sigma} \times\left\{(2+\sigma) - \frac{2\sigma\left(\frac{n}{\kappa^\sigma}+2\right)}{\left\{\frac{n}{\kappa^\sigma}+4(1-\sigma\kappa)\right\}}\right\}\Bigg] - \epsilon\left[\frac{\sigma\left(\frac{n}{\kappa^\sigma}+2\right)}{2\left\{\frac{n}{\kappa^\sigma}+4(1-\sigma\kappa)\right\}}\right] + O(\epsilon^2). \tag{26}$$

In Fig. 4, we display the variations of w with (a) n and (b) κ in three dimensions. In Fig. 4(a), we show the variations of w with n for $\kappa = 0.001$ while in Fig. 4(b) we show the variation of w with κ for $n = 3$. These plots clearly show that the dependence

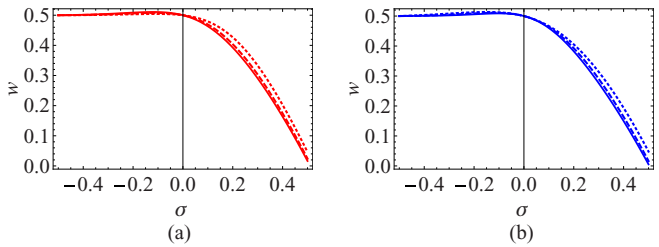

FIG. 4. Plots for $w = -\sigma + \epsilon f_2(\sigma,\kappa,n) + O(\epsilon^2)$. Panel (a) shows the variation of w with n for $\kappa = 0.001$ and panel (b) shows the variation of w with κ for $n = 3$ in $d = 3$. The dotted, dashed, and solid curves correspond to $n = 1,2,3$ in (a) and $\kappa = 0.0001, 0.001, 0.01$ in (b).

on n and κ of the linewidth exponent w is insignificant and, interestingly, $w \approx 0.5$ in the range $-0.5 < \sigma < 0$.

Further, the exponent νz, related to the characteristic time scale as $\tau \propto |T - T_c|^{-z\nu}$, is obtained as

$$\nu z = 1 + \frac{\epsilon\left(\frac{n}{\kappa^\sigma} + 2\right)}{\left\{\frac{n}{\kappa^\sigma} + 4(1 - \sigma\kappa)\right\}} \times \left\{\frac{1}{2} + \frac{2\sigma}{(\sigma + 2)\left[\frac{n}{\kappa^\sigma} + 4(1 - \sigma\kappa)\right] - 4\sigma}\right\} + O(\epsilon^2). \tag{27}$$

The other static critical exponents, namely the spontaneous magnetization exponent β, susceptibility exponent γ, and critical isotherm exponent δ, can be obtained by using the expressions for η and ν from Eqs. (23) and (25) in the well-known scaling relations, namely Josephson scaling $\nu d = 2 - \alpha$, Fisher scaling $\gamma = \nu(2 - \eta)$, Widom scaling $\gamma = \beta(\delta - 1)$, and Rushbrooke scaling $\alpha + 2\beta + \gamma = 2$ [55,57]. This yields

$$\beta = \frac{\sigma + 1}{2} - \frac{\epsilon}{4}\left[1 + \frac{2\sigma(\sigma + 2)}{(\sigma + 2)\left[\frac{n}{\kappa^\sigma} + 4(1 - \sigma\kappa)\right] - 4\sigma} - \frac{\left(\frac{n}{\kappa^\sigma} + 2\right)(2\sigma + 2)}{\frac{n}{\kappa^\sigma} + 4(1 - \sigma\kappa)} \times \left\{\frac{1}{2} + \frac{2\sigma}{(\sigma + 2)\left[\frac{n}{\kappa^\sigma} + 4(1 - \sigma\kappa)\right] - 4\sigma}\right\}\right] + O(\epsilon^2), \tag{28}$$

$$\gamma = 1 + \frac{\epsilon\left(\frac{n}{\kappa^\sigma} + 2\right)}{\frac{n}{\kappa^\sigma} + 4(1 - \sigma\kappa)}\left[\frac{1}{2} + \frac{2\sigma}{(\sigma + 2)\left[\frac{n}{\kappa^\sigma} + 4(1 - \sigma\kappa)\right] - 4\sigma}\right] + O(\epsilon^2), \tag{29}$$

and

$$\delta = \frac{\sigma + 3}{\sigma + 1} + \frac{\epsilon}{\sigma + 1}\left[\frac{1}{\sigma + 1} + \frac{2\sigma(\sigma + 2)}{(\sigma + 1)\left[(\sigma + 2)\left\{\frac{n}{\kappa^\sigma} + 4(1 - \sigma\kappa)\right\} - 4\sigma\right]}\right] + O(\epsilon^2). \tag{30}$$

III. COMPARISON WITH EXPERIMENTS

As noted earlier, in recent experimental studies on the critical behavior of perovskite manganites [16,18–21], the relaxation rate of the system near the critical point has been measured by various techniques. In Table I and II, we display the experimental results and compare them with our calculated results. To compare the results, we first match the experimental value of β with our theoretical estimate from Eq. (28) by tuning the long-range exponent σ. For the same value of σ, we then calculate the other exponents, namely γ, δ, z, w, and νz from Eqs. (29), (30), (24), (26), and (27), respectively.

Atsarkin *et al.* [20] investigated the critical slowing down of longitudinal spin relaxation close to the PM-FM critical point T_c in $La_{1-x}Ca_xMnO_3$ for $x = 0.2, 0.25, 0.33$. It is interesting to note that they measured the exponent $w \approx 0.5$ for all those samples from EPR linewidth measurements. Using a similar experimental technique, Yassin *et al.* [21] also obtained the same value ($w \approx 0.5$) for a wide range of doping levels x in $La_{0.67-2x}Nd_{2x}Ca_{0.33-x}Sr_xMnO_3$, namely $x = 0$, 0.1, 0.15, 0.2, and 0.25. These experimental estimates for w are in excellent agreement with our calculated results for w in the range $-0.5 < \sigma < 0$ as shown in Fig. 4. Thus the nonlocal model Hamiltonian governing the critical dynamics correctly captures the trend of a constant value of w for a wide range of σ akin to the wide range of x in the experimental samples. This trend appears to be true for different constituent R and A in perovskite manganites. In addition, we see from Table I that the values of β, γ, and δ for $\sigma = -0.193$ are in close agreement for the sample $La_{1-x}Ca_xMnO_3$ with $x = 0.2$ [58]. For $x = 0.33$, the β value is available in Ref. [15] and we display it in Table I. For the other doping level, namely, $x = 0.25$, the experimental estimates for static critical exponents are not available at present. Similarly, the static critical exponents for the samples $La_{0.67-2x}Nd_{2x}Ca_{0.33-x}Sr_xMnO_3$ studied in Ref. [21] are not available except for $x = 0$ [15].

Krishnamurthy *et al.* [16] performed a μSR experiment and studied the critical slowing down of Mn ion spin fluctuations in the critical paramagnetic regime in single-crystal $Nd_{0.5}Sr_{0.5}MnO_3$ and obtained $w = 0.59 \pm 0.05$. From this value of w, they estimated the value $z = 2.00 \pm 0.12$ from the scaling law $w = \nu(z + 2 - d - \eta)$, where the value $\nu = 0.61 \pm 0.02$ was taken from another experiment [59] and $\eta = 0.031 \pm 0.004$ from the RG calculation of model C [22]. In addition to the linewidth exponent w, they [16] also measured the static critical exponents β, γ, and δ. Here we compare them with our results and find that, although there is a slight departure in the w value, the values for z, β, γ, and δ are in good agreement.

In a few other experiments on perovskite manganites [18,19], direct observational values for z and w are not available. For example, Liu *et al.* [18,19] measured the relaxation time exponent $\nu z = 1.39$ for the thin-film samples

TABLE I. Comparison of the critical exponents z, w, β, γ, and δ following from Eqs. (24), (26), (28), (29), and (30) for $n = d = 3$ and $\kappa = 0.001$ with experimental estimates obtained for perovskite manganite compounds. Unavailable experimental data are indicated by dashes; PC denotes polycrystalline and SC denotes single-crystal samples.

σ	Experimental sample	Ref.	z	w	β	γ	δ
−0.148			1.979	0.510	0.345	1.201	4.264
	$La_{0.67}Ca_{0.33}MnO_3$ (PC)	[15,20,21]	–	0.50	0.345 ± 0.015	–	–
−0.193			1.975	0.509	0.328	1.164	4.351
	$La_{0.8}Ca_{0.2}MnO_3$ (SC)	[20,58]	–	0.50	0.328	1.193	4.826
−0.186			1.975	0.509	0.330	1.170	4.338
	$Nd_{0.5}Sr_{0.5}MnO_3$ (SC)	[16]	2.00 ± 0.12	0.59 ± 0.05	0.33 ± 0.02	1.24 ± 0.03	–
	$La_{0.75}Ca_{0.25}MnO_3$ (SC)	[20]	–	0.50	–	–	–
	$La_{0.47}Nd_{0.2}Ca_{0.23}Sr_{0.1}MnO_3$ (PC)	[21]	–	0.49	–	–	–
	$La_{0.37}Nd_{0.30}Ca_{0.18}Sr_{0.15}MnO_3$ (PC)	[21]	–	0.49	–	–	–
	$La_{0.27}Nd_{0.4}Ca_{0.13}Sr_{0.2}MnO_3$ (PC)	[21]	–	0.49	–	–	–
	$La_{0.17}Nd_{0.5}Ca_{0.08}Sr_{0.25}MnO_3$ (PC)	[21]	–	0.50	–	–	–

$La_{0.7}Sr_{0.3}MnO_3$ and $La_{0.7}Ca_{0.3}MnO_3$. Based on the closeness of this experimental value with the prediction of the 3D Heisenberg model, they concluded that the critical behavior of both the samples should be governed by the 3D Heisenberg model. However, in a different set of experiments on $La_{0.7}Sr_{0.3}MnO_3$ [11] and $La_{0.7}Ca_{0.3}MnO_3$ [60], it was concluded from the results of static critical exponents that the 3D Heisenberg model is not adequate enough to describe their critical behavior. This casts some doubt on the applicability of the 3D Hesisenberg model on these samples. It is important to note that this disagreement in the experimental results, despite the same chemical composition of the two samples, is most likely due to the difference in their physical forms in these two experiments. In Refs. [18,19], the samples were thin films of thicknesses ~ 200 nm, whereas in Refs. [11,60] the experiments were performed on bulk samples. Consequently, it is expected that the finite-size effects will play some role in determining the critical behavior in the thin-films case. It is apparent that the experimental measurements on the thin films did not take this finite-size effect into consideration and, as a result, the corresponding critical exponents cannot be expected to agree with those coming from the bulk samples. As we see from Table II, although our theoretical values for the critical exponents β, γ, and δ agree well with the experimental ones, the value of νz does not agree too well with the thin-film measurements. We cannot expect a good agreement with the thin-film samples because our results are applicable for bulk samples without any finite-size effects.

IV. DISCUSSIONS AND CONCLUSIONS

In this paper, we have performed a dynamic RG analysis on the dynamic model [Eq. (1)] governed by the nonlocal model Hamiltonian [Eq. (2)]. Carrying out the calculations at one-loop order in the leading order of $\epsilon = 4 - d + 2\sigma$, we have seen that the nontrivial fixeded point is stable in the range $-0.5 \leqslant \sigma \leqslant 0.5$ in three dimensions. Within this range of σ, our present model Hamiltonian yields nonzero values of the Fisher exponent η, giving $z = 2 + \epsilon f_1(\sigma,\kappa,n) + O(\epsilon^2)$. The plots for z in three dimensions given in Fig. 3 indicate that their dependencies on the model parameters n and κ are insignificant in the negative range of σ. It may be noted that the dynamic exponent lies in the range $1.972 \leqslant z \leqslant 2.016$ for $n = 3$ in three dimensions. We have derived an expression [Eq. (26)] for the linewidth exponent w in the leading order of ϵ yielding $w = -\sigma + \epsilon f_2(\sigma,\kappa,n) + O(\epsilon^2)$. This leads to $w \approx 0.5$ in three dimensions in the range $-0.5 \leqslant \sigma \leqslant 0$ irrespective of the values of the model parameters n and κ, as shown in Fig. 4. This is consistent with the experimental investigations [20,21], suggesting that the linewidth exponent w for perovskite manganite samples has an almost constant value $w \approx 0.5$ irrespective of their chemical compositions. A few experiments studying the dynamic critical behavior of perovskite manganites measured the value of the relaxation time exponent νz. Consequently, we calculated its value leading to $\nu z = 1 + \epsilon f_3(\sigma,\kappa,n) + O(\epsilon^2)$ at one-loop order. The currently available experimental estimates for the exponents w and νz lie well within the range $-0.5 \leqslant \sigma \leqslant 0$, as shown in Table I and

TABLE II. Comparison of the critical exponents νz, β, γ, and δ following from Eqs. (27), (28), (29), and (30) for $n = d = 3$ and $\kappa = 0.001$ with experimental estimates obtained for perovskite manganite compounds.

σ	Experimental sample	Ref.	νz	β	γ	δ
−0.094			1.251	0.370	1.251	4.164
	$La_{0.7}Sr_{0.3}MnO_3$ (SC)	[18]	1.39	–	–	–
	$La_{0.7}Sr_{0.3}MnO_3$ (SC)	[11]	–	0.37 ± 0.04	1.22 ± 0.03	4.25 ± 0.2
−0.114			1.232	0.360	1.232	4.201
	$La_{0.7}Ca_{0.3}MnO_3$ (SC)	[19]	1.39 ± 0.06	–	–	–
	$La_{0.7}Ca_{0.3}MnO_3$ (SC)	[60]	–	0.36 ± 0.01	1.2	4.263

Table II. In addition, as displayed in Table I, within the same stable range of the nontrivial fixed point, the present nonlocal model Hamiltonian reproduces satisfactorily the static critical exponents for the samples for which experimental values of the linewidth exponent are also available from various spin relaxation experiments [16,20,21]. It is worth noting that in Refs. [20,21] the value of $w = 0.5$ was obtained from the EPR linewidth for various doping levels x. The measured static critical exponents β, γ, and δ in the available experiments [15,58] are also presented in Table I and they agree well with the present theoretical estimates. However, the estimates coming from μSR experiment [16] yields $w \approx 0.59$. This value, although, slightly deviates from our model predictions ($w \approx 0.5$), and the other critical exponents z, β, and γ obtained in the same experiment [16] are in good agreement.

Further, while comparing the relaxation exponent νz in Table II with the available experimental estimates [18,19], we observed a slight mismatch which appears to be a consequence of finite-size effects for which one expects finite-size corrections in the thin-film samples, as discussed earlier in Sec. III. However, the static critical exponents for the same (bulk) samples, as available in Refs. [11,60], match well with our model predictions as displayed in Table II.

We have thus seen that our theoretical predictions for the critical exponents are in reasonable agreement with the experimental ones considering that our calculations are at one loop order. We expect, as in the standard ϕ^4 theory [61], better agreements with the critical exponents if the calculations are performed up to two-loop order. Moreover, just like in the standard ϕ^4 theory, to get very precise values of the critical exponents one needs to calculate the Feynman diagrams up to five- or six-loop orders and perform a Borel summation of the resulting ϵ expansion [62]. We deem such a detailed and more exact calculation unnecessary because our calculations capture the correct trend of the static and dynamic critical exponents already at one loop order that helps us to ascertain about the form of the nonlocal interaction in the effective Hamiltonian.

In this context, we would like to note from a number of previous theoretical investigations [50,52], that nonlocal interaction in the effective Hamiltonian emerges in systems involving spin-lattice coupling. In particular, Fisher [49] considered spin-lattice coupling in a compressible Ising system by accounting for the fact that the exchange interaction varies with the separation between the spins. Reconsidering this problem, Wagner [50] showed the emergence of nonlocal four spin interaction in the effective spin Hamiltonian. Aharony considered a continuum generalization of this Hamiltonian and predicted the existence of tricriticality in the system [52]. It is thus interesting to investigate whether nonlocal interactions are capable of reproducing the wide range of universality classes (apart from tricriticality) observed in perovskite manganites that are known to possess a strong spin-lattice coupling. In fact, an effective Hamiltonian with nonlocal interaction in the quartic term was analyzed via Wilson's momentum shell decimation RG scheme. It was found that the model could reproduce a vast range of static critical properties including tricriticality in a satisfactory manner for widely varying compositions of experimental samples [53]. Remarkably, the dynamic critical behavior of the (experimentally explored) perovskite manganites gives clear indication that the linewidth exponent remains approximately constant, although their static critical exponents vary across samples. It is gratifying that the nonlocal model considered in this paper is capable of reproducing the correct trends of both static and dynamic critical exponents observed in experimental perovskite manganite samples.

We conclude by noting that the critical behavior near the second-order phase transition in CMR materials has been extensively explored in the recent past due to their high technological demands. Since there has been a great deal of experimental data on the critical behavior of these systems, it is an interesting adventure to explore them on theoretical grounds. The nonlocal model in this work is only an initial theoretical attempt to describe their dynamic critical behavior. It is, however, worth remarking that a very few experimental works on the dynamic critical behavior of perovskite manganites have been reported in comparison to the enormous number of static critical measurements. Additional experimental investigations on the dynamic critical behavior will be required to verify the model predictions. Particularly, the dynamic exponents need to be measured for varying compositions of perovskite manganite samples. We hope that the present work will inspire to carry out further experimental research along this line.

ACKNOWLEDGMENTS

R.S. is thankful to the Ministry of Human Resource Development (MHRD), Government of India, for financial support through a scholarship. M.K.N. is indebted to the Indian Institute of Technology Delhi, and particularly to Professor Ravisankar and Professor Senthilkumaran, for hospitality at I.I.T. Delhi.

[1] B. I. Halperin and P. C. Hohenberg, Phys. Rev. Lett. **19**, 700 (1967).
[2] B. I. Halperin and P. C. Hohenberg, Phys. Rev. **177**, 952 (1969).
[3] B. I. Halperin, P. C. Hohenberg, and S.-k. Ma, Phys. Rev. Lett. **29**, 1548 (1972).
[4] B. I. Halperin, P. C. Hohenberg, and S.-k. Ma, Phys. Rev. B **10**, 139 (1974).
[5] B. I. Halperin, P. C. Hohenberg, and S.-k. Ma, Phys. Rev. B **13**, 4119 (1976).
[6] P. C. Hohenberg and B. I. Halperin, Rev. Mod. Phys. **49**, 435 (1977).
[7] G. F. Mazenko, *Nonequilibrium Statistical Mechanics* (Wiley-Vch, Weinheim, 2006).
[8] M. E. Fisher, S.-k. Ma, and B. G. Nickel, Phys. Rev. Lett. **29**, 917 (1972).

[9] S. V. Belim, JETP Lett. **98**, 745 (2004).
[10] A. J. Millis, Nature (London) **392**, 147 (1998).
[11] K. Ghosh, C. J. Lobb, R. L. Greene, S. G. Karabashev, D. A. Shulyatev, A. A. Arsenov, and Y. Mukovskii, Phys. Rev. Lett. **81**, 4740 (1998).
[12] N. A. Babushkina, L. M. Belova, O. Y. Gorbenko, A. R. Kaul, A. A. Bosak, V. I. Ozhogin, and K. I. Kugel, Nature (London) **391**, 159 (1998).
[13] M. B. Salamon and M. Jaime, Rev. Mod. Phys. **73**, 583 (2001).
[14] E. Dagotto, *Phase Seperation and Colossal Magnetoresistance* (Springer, Berlin, 2002).
[15] R. H. Heffner, L. P. Le, M. F. Hundley, J. J. Neumeier, G. M. Luke, K. Kojima, B. Nachumi, Y. J. Uemura, D. E. MacLaughlin, and S.-W. Cheong, Phys. Rev. Lett. **77**, 1869 (1996).
[16] V. V. Krishnamurthy, I. Watanabe, K. Nagamine, H. Kuwahara, and Y. Tokura, Phys. Rev. B **61**, 4060 (2000).
[17] L. V. Doloc, J. W. Lynn, Y. M. Mukovskii, A. A. Arsenov, and D. A. Shulyatev, J. Appl. Phys. **83**, 7342 (1998).
[18] X. J. Liu, Y. Moritomo, A. Nakamura, H. Tanaka, and T. Kawai, J. Phys. Soc. Jpn. **70**, 3466 (2001).
[19] X. J. Liu, Y. Moritomo, A. Nakamura, H. Tanaka, and T. Kawai, Phys. Rev. B **64**, 100401(R) (2001).
[20] V. A. Atsarkin, V. V. Demidov, G. A. Vasneva, and K. Conder, Phys. Rev. B **63**, 092405 (2001).
[21] O. A. Yassin, M. I. Mohamed, and S. N. Bhatia, Phys. Status Solidi B **245**, 745 (2008).
[22] C. Hohenemser, N. Rosov, and A. Kleinhammes, Hyperfine Interact. **49**, 267 (1989).
[23] C. Zener, Phys. Rev. **82**, 403 (1951).
[24] H. A. Jahn and E. Teller, Proc. R. Soc. London A **161**, 220 (1937).
[25] A. J. Millis, B. I. Shraiman, and R. Mueller, Phys. Rev. Lett. **77**, 175 (1996).
[26] A. Shengelaya, G.-M. Zhao, H. Keller, and K. A. Müller, Phys. Rev. Lett. **77**, 5296 (1996).
[27] A. Shengelaya, G.-M. Zhao, H. Keller, K. A. Müller, and B. I. Kochelaev, Phys. Rev. B **61**, 5888 (2000).
[28] A. A. Caparica, A. Bunker, and D. P. Landau, Phys. Rev. B **62**, 9458 (2000).
[29] Y. Motome and N. Furukawa, J. Phys. Soc. Jpn. **69**, 3785 (2000).
[30] Y. Motome and N. Furukawa, J. Phys. Soc. Jpn. **72**, 2126 (2003).
[31] Y. Motome and N. Furukawa, Phys. Rev. B **68**, 144432 (2003).
[32] H. A. Fernandes, J. R. Drugowich de Felício, and A. A. Caparica, Phys. Rev. B **72**, 054434 (2005).
[33] K. Chen, A. M. Ferrenberg, and D. P. Landau, Phys. Rev. B **48**, 3249 (1993).
[34] C. Holm and W. Janke, Phys. Rev. B **48**, 936 (1993).
[35] S. Nair, A. Banerjee, A. V. Narlikar, D. Prabhakaran, and A. T. Boothroyd, Phys. Rev. B **68**, 132404 (2003).
[36] B. Padmanabhan, H. L. Bhat, S. Elizabeth, S. Rößler, U. K. Rößler, K. Dörr, and K. H. Müller, Phys. Rev. B **75**, 024419 (2007).
[37] M. C. Martin, G. Shirane, Y. Endoh, K. Hirota, Y. Moritomo, and Y. Tokura, Phys. Rev. B **53**, 14285 (1996).
[38] C. S. Hong, W. S. Kim, and N. H. Hur, Phys. Rev. B **63**, 092504 (2001).
[39] D. Kim, B. Revaz, B. L. Zink, F. Hellman, J. J. Rhyne, and J. F. Mitchell, Phys. Rev. Lett. **89**, 227202 (2002).
[40] R. Venkatesh, M. Pattabiraman, K. Sethupathi, G. Rangaragan, S. Angappane, and J.-G. Park, J. Appl. Phys. **103**, 07B319 (2008).
[41] J. Fan, L. Ling, B. Hong, L. Zhang, L. Pi, and Y. Zhang, Phys. Rev. B **81**, 144426 (2010).
[42] H. Y. Hwang, S.-W. Cheong, P. G. Radaelli, M. Marezio, and B. Batlogg, Phys. Rev. Lett. **75**, 994 (1995).
[43] R. P. Sharma, G. C. Xiong, C. Kwon, R. Ramesh, R. L. Greene, and T. Venkatesan, Phys. Rev. B **54**, 10014 (1996).
[44] C. H. Booth, F. Bridges, G. H. Kwei, J. M. Lawrence, A. L. Cornelius, and J. J. Neumeier, Phys. Rev. Lett. **80**, 853 (1998).
[45] G.-M. Zhao, K. Konder, H. Keller, and K. A. Müller, Nature (London) **381**, 676 (1996).
[46] A. J. Millis, T. Darling, and A. Migliori, J. Appl. Phys. **83**, 1588 (1998).
[47] K. H. Ahn, T. Lookman, and A. R. Bishop, Nature **428**, 401 (2004).
[48] D. I. Khomskii and K. I. Kugel, Phys. Rev. B **67**, 134401 (2003).
[49] M. E. Fisher, Phys. Rev. **176**, 257 (1968).
[50] H. Wagner, Phys. Rev. Lett. **25**, 31 (1970).
[51] H. Wagner and J. Swift, Z. Phys. **239**, 182 (1970).
[52] A. Aharony, Phys. Rev. B **8**, 4314 (1973).
[53] R. Singh, K. Dutta, and M. K. Nandy, Phys. Rev. E **92**, 012123 (2015).
[54] S.-k. Ma, *Modern Thoery of Critical Phenomena* (Benjamin, Reading, MA, 1976).
[55] N. Goldenfeld, *Lectures on Phase Transitions and the Renormalization Group* (Addison-Wesley, Reading, MA, 1992).
[56] H. E. Stanley, *Introduction to Phase Transitions and Critical Phenomena* (Oxford University Press, New York, 1971).
[57] D. J. Amit and V. Martin-Mayor, *Field Theory, the Renormalization Group, and Critical Phenomena*, 3rd ed. (World Scientific, Singapore, 2005).
[58] M. Khlifi, A. Tozri, M. Bejar, E. Dhahri, and E. K. Hlil, J. Magn. Magn. Mater. **324**, 2142 (2012).
[59] S. Rosenkranz, R. Osborn, J. F. Mitchell, U. Geiser, J. Ku, A. J. Schultz, and D. M. Young, Physica B **241-243**, 448 (1998).
[60] S. Taran, B. K. Chaudhuri, S. Chatterjee, H. D. Yang, S. Neeleshwar, and Y. Y. Chen, J. Appl. Phys. **98**, 103903 (2005).
[61] K. G. Wilson and J. Kogut, Phys. Rep. **12**, 75 (1974).
[62] H. Kleinert and V. Schulte-Frohlinde, *Critical Properties of ϕ^4-Theories* (World Scientific, Singapore, 2001).